Ocean Engineering 37 (2010) 491–497

Contents lists available at ScienceDirect

Ocean Engineering

journal homepage: www.elsevier.com/locate/oceaneng

A numerical model for predicting the jump of lift force on an oscillating cylinder

Li Lei, Lin Mian *

Laboratory of Environment Mechanics, Institute of Mechanics, Chinese Academy of Sciences, Beisihuan Road 15, Haidian District, Beijing 100190, China

ARTICLE INFO

Article history:
Received 24 February 2009
Accepted 24 January 2010
Available online 4 February 2010

Keywords:
Oscillating cylinder
Lift jump
Large eddy simulation

ABSTRACT

The fluid force coefficients on a transversely oscillating cylinder are calculated by applying two-dimensional large eddy simulation method. Considering the "jump" phenomenon of the amplitude of lift coefficient is harmful to the security of the submarine slender structures, the characteristics of this "jump" are dissertated concretely. By comparing with experiment results, we establish a numerical model for predicting the jump of lift force on an oscillating cylinder, providing consultation for revising the hydrodynamic parameters and checking the fatigue life scale design of submarine slender cylindrical structures.

1. Introduction

The alternating lift force induced by periodic vortex shedding from submarine structures can evidently diminish their fatigue life. A large amount of experiments have focused on this problem (Sarpkaya, 1978, 1995; Staubli, 1983; Gopalkrishnan, 1993; Govardhan and Wiliamson, 2000; Carberry et al., 2005). It is found that an abrupt change will present in amplitude and phase of the fluid forces, especially the lift force, as the frequency f_e of a transversely oscillating circular cylinder is close to the Strouhal frequency f_0 of a fixed cylinder. According to the observation in experiments, the jump in phase of lift and drag at transition is relatively independent of the two variables: oscillation frequency and Reynolds number, while the jump in magnitude of lift force depends on both variables. The jump in lift force can induce variation of the stress states which would reduce the lifespan of submarine structures such as free spanning pipelines, anchor chains, riser and so on. Thus the effect of those parameters on lift force is a key issue for scientists and engineers.

Some numerical studies have been accumulated for the last over-10 years. (Lu and Dalton, 1996) investigated the vortex shedding from a transversely oscillating circular cylinder in a uniform flow by solving two dimensional unsteady *N–S* equations with three Reynolds numbers: 185, 500 and 1000. The primitive-variable formulation and a staggered grid, spaced in the circumferential direction uniformly and stretched in the radial direction exponentially, are employed for computing the flow field. Anagnostopoulos (2000) dealt with the problem using finite element method and found corresponding changes in the hydrodynamic forces and the parameters of the wake geometry. Leontini et al. (2005) performed a two-dimensional simulation at a Reynolds number of 200 and employed spectral-element method for two cases: an elastically mounted cylinder and an externally driven oscillating cylinder. The results showed that the driven oscillating system is highly sensitive to the amplitude and frequency of oscillation. Jamal and Dalton (2005) investigated the difference of phase angles of fluid forces in forced and self-excited oscillations of a circular cylinder at Re=8000 applying a 2D LES method. His calculation indicates the LES is able to simulate the complex wake modes downwards the oscillating cylinder such as 2P, 2S and P+S. Kaiktsis et al. (2007) considered a harmonic oscillating cylinder in the direction perpendicular to a uniform flow by solving the two dimensional Navier–Stokes equation at Re=400. Qualitative differences are found between the results of the below resonance and the resonant or above resonance forcing.

In this paper, a novel optimized mesh configuration is used to perform a large eddy simulation for simulating the force states of a transversely oscillating cylinder in a range of moderate Reynolds numbers. Some satisfactory results are obtained by comparison with the former experimental data by Carberry et al. (2005). Analysis of the results with respect to a free spanning pipeline provides more and significant cognition of the hydrodynamic forces acting on the submarine structures. Based on the correct results obtained from the computational model, this numerical lift jump model can be valid to predict the variation of lift force jump within a certain range of Reynolds number as the referred experiment, which is a beneficial complementarity for the present ocean engineering structure code of design and assessment.

2. Numerical model

We consider the case of a circular cylinder undergoing a sinusoidal oscillation perpendicular to the uniform approach flow

* Corresponding author. Tel.: +86 10 82544206.
E-mail address: linmian@imech.ac.cn (L. Mian).

0029-8018/$ - see front matter © 2010 Elsevier Ltd. All rights reserved.
doi:10.1016/j.oceaneng.2010.01.010

(Fig. 1). The displacement equation of the cylinder is given as

$$\vec{y} = A\sin(2\pi f_e t) \tag{1}$$

where A is the amplitude and set a constant value of 0.5D in our study, D is the diameter of the cylinder, f_e is the oscillation frequency and the variable $\boldsymbol{t}$ denotes time.

Assuming the approach flow as incompressible and viscous, the stream function $\boldsymbol{\psi}$ is governed by the Poisson equation:

$$\nabla^2\psi = -\omega \tag{2}$$

and the two-dimensional vorticity equation is written as

$$\frac{\partial\omega}{\partial t} + u\frac{\partial\omega}{\partial r} + \frac{v}{r}\frac{\partial\omega}{\partial\theta} = (\upsilon+\upsilon_t)\left(\frac{\partial^2}{\partial r^2} + \frac{1}{r}\frac{\partial}{\partial r} + \frac{\partial^2}{\partial\theta^2}\right)\omega \tag{3}$$

In these equations, $\nabla^2 = \frac{\partial^2}{\partial r^2} + \frac{1}{r}\frac{\partial}{\partial r} + \frac{\partial^2}{\partial\theta^2}$ represents the Laplacian under polar coordinates, $\omega = \frac{1}{r}\frac{\partial(rv)}{\partial r} - \frac{1}{r}\frac{\partial(u)}{\partial\theta}$ is vorticity of the whole flow field. $u = \frac{1}{r}\frac{\partial\psi}{\partial\theta}$ and $v = -\frac{\partial\psi}{\partial r}$ are the radial and circumferential components of velocity, respectively, υ is the kinetic viscosity coefficient of fluid, $\upsilon_t (= (C_s\Delta)^2\sqrt{2S_{ij}S_{ij}})$, defined by Smagorinsky subgrid scale mode, is the turbulence eddy viscosity coefficient, where $C_s\Delta$ is the mixed length, C_s the Smagorinsky constant (Zhang et al., 2008), Δ the scale of filter and S_{ij} the tensor of strain rate.

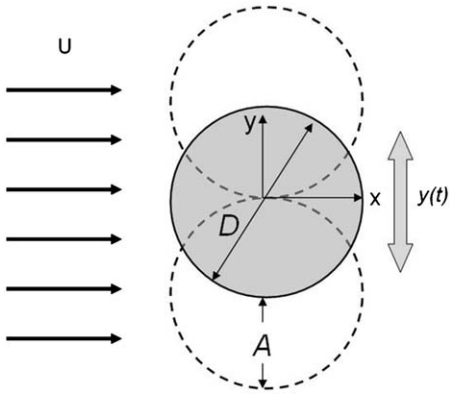

Fig. 1. Sketch of the cylinder motion.

The diameter of the cylinder D and the velocity of incoming flow U_∞ are designated to be the characteristic variables. Then the dimensionless governing equation can be written as

$$\frac{\partial\omega}{\partial\tau} + u\frac{\partial\omega}{\partial r} + \frac{v}{r}\frac{\partial\omega}{\partial\theta} = \left(\frac{2}{Re} + \frac{2}{Re_t}\right)\nabla^2\omega \tag{4}$$

where $\tau = tU_\infty/R$, dimensionless time; $Re = U_\infty R/\upsilon$ and $Re_t = U_\infty R/\upsilon_t$.

Owing to the oscillation of cylinder, the dynamic mesh technique is applied to the process of computation. The optimal mesh configuration of the computational domain is finally determined by several numerical testing as shown in Fig. 2a and b. In order to indicate the superiority of the final optimized mesh configuration, the mesh configuration of a testing model is shown in Fig. 2c as comparison. The grid partition near the cylinder of the final mesh is different from the testing one (Fig. 2c). The grid type of the testing model outside the cylinder is completely nonstructural triangle cell, which can be deforming with the motion of the cylinder wall. In the final model, the computational domain is divided into three sub-regions according to different mesh principles. The first sub-region is near-cylinder region, which has the same motion style as the cylinder boundary. This region is constituted by quadrangular structural grid. The relative locations of the nodes are invariable. The second one around the near-cylinder region with triangular nonstructural grid is called "inner zone", which would be deformed or remeshed due to the motion of cylinder and near-cylinder region. Outside the inner zone, it is the outer zone, whose elements are quadrangular structural and ametabolic. The application of dynamic mesh technique includes two steps: spring smoothing and local remeshing. The borders of cells in the inner zone may be stretched or compressed like springs when the cylinder is

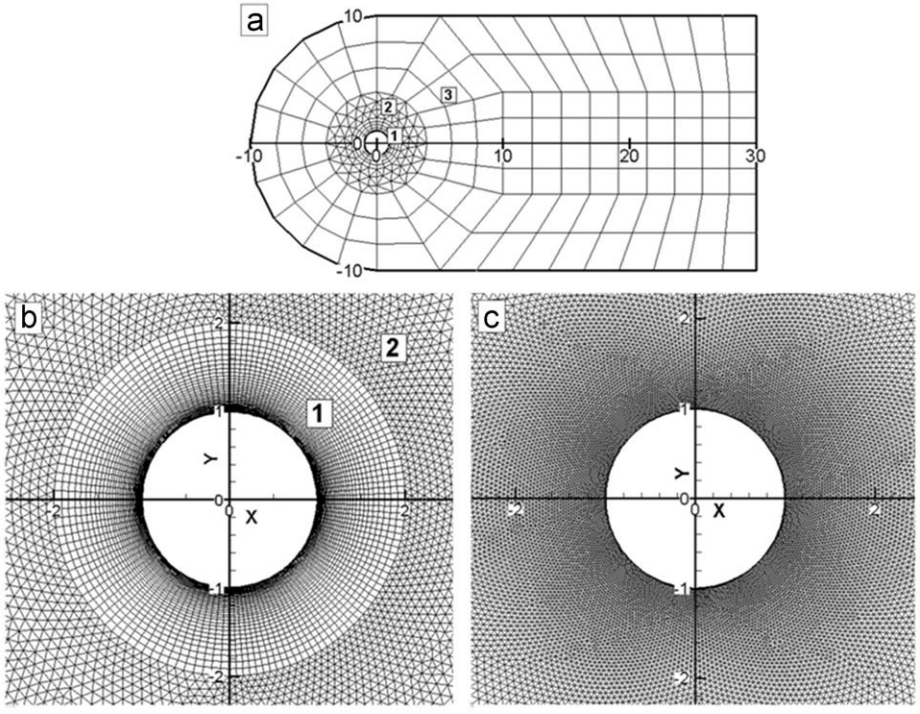

Fig. 2. Mesh skeleton and configuration of the computational domain: (a) mesh skeleton of the final model, (b) details around the cylinder of the final mesh and (c) details around the cylinder of the test mesh; 1, near cylinder region, 2, inner zone, 3, outer zone.

oscillating. Three limens: the maximum cell skewness, the minimum and the maximum cell area are predefined to determine the cells whether to be stretched, compressed subsequently or remeshed drastically.

In the computational domain, the left-hand inflow boundary is assumed to have a uniform velocity according to the flow Reynolds number. The upper and bottom boundaries are the same as the left-hand inflow boundary. The right-hand boundary is set to be pressure out-let, for which a zero-derivative continuative boundary condition is used. The cylinder surface is assumed to be non-slip and hydraulically smooth.

3. Results and discussions

In order to enhance the computational precision and to obtain the optimal mesh configuration, we take the experimental results of (Carberry et al., 2005) as references. The cases we calculated are divided into three groups according to different Reynolds numbers, in which 2300, 4410 and 9100 are the same as the related experiments. In each case, the oscillation amplitude of cylinder is constant. The frequency ratio α (f_e/f_0) in each group is different according to different sensitivity to the emergence of the force jump phenomenon during the computation process (Table 1).

3.1. Data post-processing

The time history of lift coefficient acting on the cylinder can be ultimately obtained. It is composed by componential signals with different frequencies. In order to study the property of the lift clearly, Fourier analysis should be adopted. Fig. 3a is the frequency spectrogram of the lift signal in a specified case whose Reynolds number is 2300. The horizontal axis is the frequency range of lift, while the vertical axis is the corresponding amplitude. The primary peak appears at the location of the oscillation frequency f_e, while the frequency ratio α is 1.086. It means that the Strouhal frequency f_0 is very close to f_e, which can be regarded as a "synchronization" phenomenon. In the study by Carberry et al. (2005), the wake is "locked on" to the cylinder oscillation and the dominant frequency in the lift forces is also f_e. Moreover, it is found that in all cases the correlation of the lift signal obtained from experiment with a sinusoid is greater than 0.6. Thus, the lift force can be approximated by a sinusoidal function of the form

$$Lift(t) \approx 0.5\rho U^2 DLC_L(t) = \rho U^2 DLC_L \sin(2\pi f_e t + \phi_{lift}) \quad (5)$$

where $C_L(t)$ is the fluctuating lift force coefficient, C_L the amplitude of the lift component with the frequency f_e and ϕ_{lift} the phase delay with respect to the cylinder's displacement. The subsequent analysis of the lift jump phenomenon is based on this definition of C_L. In order to compare with the experimental data, a narrow band filtering should be carried out to separate the dominant lift component with the frequency of f_e. The solid line in Fig. 3b is the history of lift component with the dimensionless frequency between 1.08 and 1.09. It will be seen that the amplitude of the lift signal is more stable with the application of the filtering process. It is more convenient for the farther analysis. Thus, the lift force can be approximated by a sinusoidal function as formula (5).

Table 1
The cases calculated with different parameters.

Re	2300	4410	9100
A/D	0.5	0.5	0.5
	0.5	0.6	0.6
	0.6	0.8	0.8
	0.7	0.85	0.85
	0.8	0.9	0.9
a	0.825	0.95	0.95
	0.85	1	1
	0.9	1.2	1.2
	0.95		
	1		
	1.2		

3.2. Optimal mesh configuration

Using the same filtering process, the lift coefficient corresponding to the frequency f_e of each case can be obtained. Results of a testing model with nonstructural mesh near the cylinder wall (Fig. 2c) are shown together with the ones of the final model in

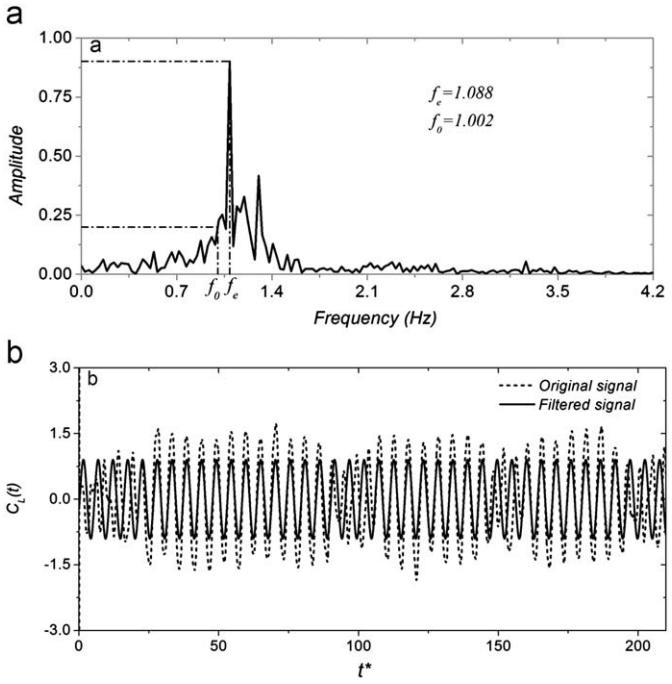

Fig. 3. (a) The frequency spectrogram of the original lift signal. (b) The original lift signal and the filtered signal.

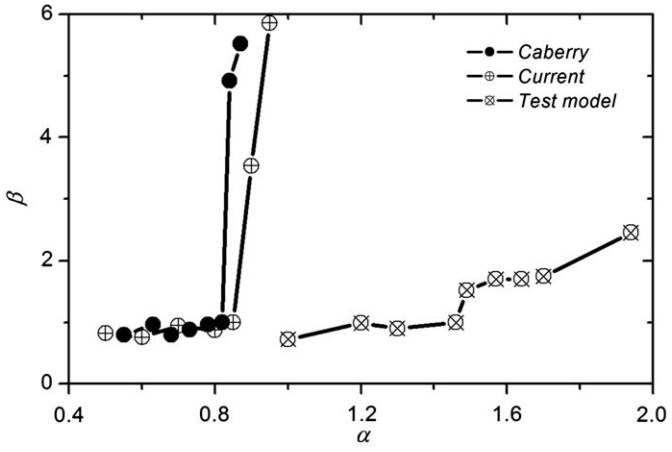

Fig. 4. Results of the final model and a testing one.

Fig. 4. The vertical axis is the normalized lift coefficient which is defined as

$$\beta = C_L/C_{LC} \tag{6}$$

It indicates the range of lift coefficient before and after the jump. C_{LC} is the last lift coefficient at the low-frequency state when α increases at the critical frequency just before lift jump. The scenario of lift jump phenomenon, which is characterized by the abrupt increase of the lift amplitude, is calculated in the final computational model with the similar parameters of C_{LC} and β as the experiment by Carberry et al. (2005).

The mesh configuration of the final model, through our computation testing, has at least two merits. First, it is more precise for the near cylinder flow calculation, which is essential for calculating the fluid forces. For the testing mesh, because the mesh near the cylinder wall would be redrawn at every time step and the relative locations of the first row of nodes to the wall are randomly distributed, the computational precision of boundary layer and its separation, even the weak flow adhering to the wall cannot be preserved. As a result of the complicated relation between jump transition and the wake mode, only guaranteeing the accuracy and precision of flow field calculation can capture the phenomenon of lift jump identical with the experimental measurements. Second, the final model is more time saving. While the dynamic mesh is carried out in the inner zone in which grid size are mostly ten times larger than those near cylinder, a larger time step can be chosen. For 200 dimensionless time history, the final model can save about 70% of the machine time than testing model.

Subsequently, a specified validity is carried out. For one thing, we name the lift coefficient at the low-frequency state as C_{LL}. When Reynolds number is 2300, the C_{LL} obtained by the final computational model are compared with the results measured in the experiment by Carberry et al. (2005) in Fig. 5. As can be seen, the C_{LL} are identical with the experimental data satisfactorily, which can be regarded as a testification for our numerical model.

3.3. Force analysis for free spanning pipelines

Considering a section of submarine free spanning pipeline, as the ocean current passes, the vortex-induced vibration (VIV) is very convenient to happen if the length of free span or the reduced velocity ($V_r=U/f_nD$) is large enough. When the VIV takes place, there are two kinds of forces acting on the free span: the in-line drag force and the cross-flow lift force. We process the time histories of lift and drag signal using the narrow band filtering simultaneously and obtain the componential signal with the oscillation frequency of free span. Then, we intercept an arbitrary period of the C_L and the corresponding two periods of the C_D and make C_D as x-coordinate and C_L as y-coordinate. The vector end of the resultant fluid forces can be drawn on the drag–lift plane. We take the cases of the low-frequency state with three different Reynolds number for example as shown in Fig. 6.

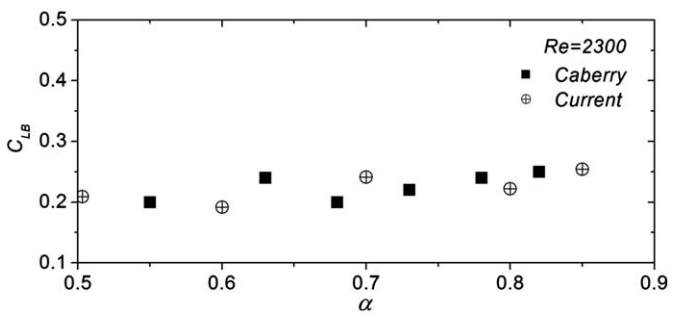

Fig. 5. Lift coefficient at low-frequency state.

We can see the fluctuating amplitude, the mean value and the relative phase angle variation of C_D and C_L. The dashed dot lines in the plane are denoting the mean lift and drag coefficients. It is obvious that the mean lift coefficient is constantly zero and the amplitude of fluctuating drag coefficient is about 0.05 in three cases with different Reynolds number. However, the amplitude of fluctuating lift coefficient is around 0.3 in the cases of Re=2300 and Re=4410 and rises distinctly to 0.5 in the case of Re=9100. Moreover, the mean drag coefficient is below 1.2 in the first two cases and exceeds this value when Re=9100.

The resultant trace of force coefficients can also demonstrate the diversification of force state of the free spanning pipeline in current. In the case of Re=2300, the maximum values of the lift and drag do not come forth at the same time. But in the case of Re=4410, it can be seen that the lift and drag achieve the maximum values simultaneously. In the case of Re=9100, when the drag achieves the maximum, the lift is zero. While the lift achieves the maximum, the drag is the minimum.

The maxima C_{max} are portrayed on the trace of drag and lift coefficients. For the flexibility of pipeline, the maximum stress should appear at the bottom of the pipeline cross-section when there are no ocean current induced forces. When the eddy induced or internal wave induced current makes the free span oscillating, the relatively dangerous state is the scenario that the resultant approaching the vertically downwards direction. We can see the downwards angle of the maximal resultant θ is more and more big in three case. The θ is defined as

$$\theta = \arctan\left(\frac{|C_{Lm}|}{|C_{Dm}|}\right)$$

where C_{Lm} and C_{Dm} are the corresponding lift and drag coefficient components when the resultant reaches maxima. Although the lift and drag coefficients cannot achieve the maximum values at the same time in the case of Re=9100, the maxima is still the largest one among the three cases because of a much more amplitude of lift and mean drag coefficient. Table 2 shows the maxima, C_{Lm} and C_{Dm}. We can see that the lift plays an important role to incense the maximum.

3.4. Analysis of the lift jump of the numerical model

According to the study by Lu and Dalton (1996), as the frequency of excitation of the cylinder increases relative to the inherent vortex formation frequency, the initially formed concentration of vorticity moves closer to the cylinder until a limiting position is reached. When this happens, the vorticity concentration abruptly switches to the opposite side of the cylinder. This process induces distinct changes of the forces acting on the cylinder. Moreover, the results of numerical study by Leontini et al. (2005) have shown that the driven oscillating system is highly sensitive to the oscillation amplitude and frequency. Changing the order of 1% in either of them two can change the magnitude of the energy transfer coefficient by the order of 25%. In Fig. 7, the similar phenomenon can be observed from the present numerical model as the hollow symbols shown.

In the present code for pipelines or risers design and safety assessment, the internal stress of the structure is evaluated by the empirical relation between the oscillation amplitude and several environmental parameters, such as reduced velocity, KC number, current wave ratio and so on. However, the external force state is the dominant condition for the structure stress calculation. In the habitual sea condition and the stationary structure, the hydrodynamic forces acting on it is relatively well known. With the weather disaster more and more frequent, the most interesting

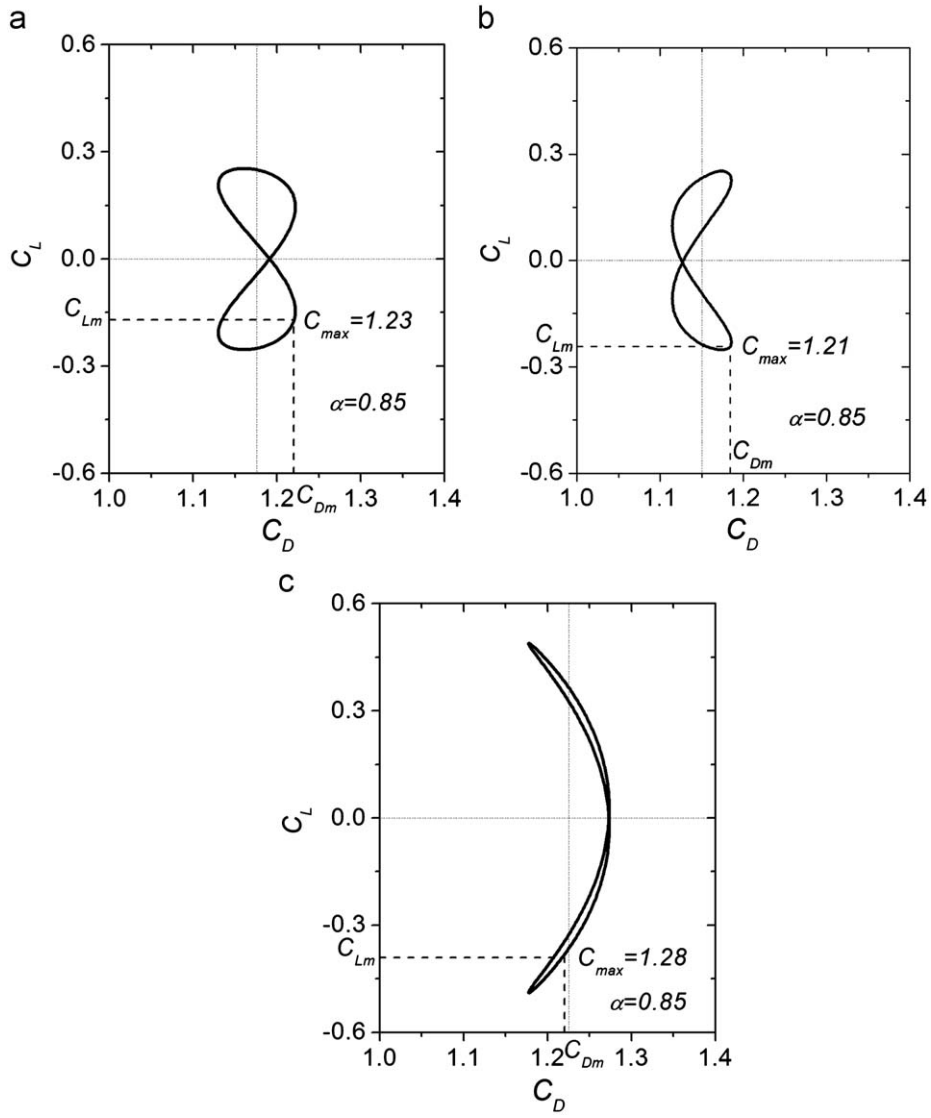

Fig. 6. (a) Force trace at *Re*=2300, (b) force trace at *Re*=4410 and (c) force trace at *Re*=9100.

Table 2
Magnitude and downwards angle of the maximum resultant and the corresponding lift drag coefficients.

Reynolds number	2300	4410	9100
C_{max}	1.23	1.21	1.28
C_{Lm}	−0.17	−0.24	−0.39
C_{Dm}	1.22	1.18	1.22
θ	7.93°	11.50°	18.29°

issue for the engineers may be the difference of force state in the extreme loading situation such as VIV resonance. This is why the lift coefficients are normalized by the C_{LC}. Next, some useful analysis and conclusions will be drawn out referred to the increase of the normalized lift coefficient after the jump occurrence.

We define the normalized lift coefficient just after the jump happens as "jump ratio" β_J. This physical parameter can determinately indicate the amplitude of the jump of lift coefficient. In the experiment by Carberry et al. (2005) and our numerical model, the jump ratio decreases with the increase of Reynolds number showed in Fig. 7. Table 3 lists the variation status of the β_J of each case with comparison to experimental data.

We choose $Re' = Re \times 10^{-3}$ as the scale of *x*-coordinate. We find that the β_J shows a very good linear relation to Re' (Fig. 8). A simple formula with the independent variable of Re' is found to describe the law of the lift jump phenomenon:

$$\beta_J = -0.55Re' + 7.08$$

This numerical result can easily be used to predict the lift jump magnitude of a structure among the Reynolds numbers of 2300–9100.

4. Conclusion

The fluid force acting on an oscillating cylinder has been calculated and analyzed in the present study. Through the force state analysis on a piece of a free spanning pipeline adopting the

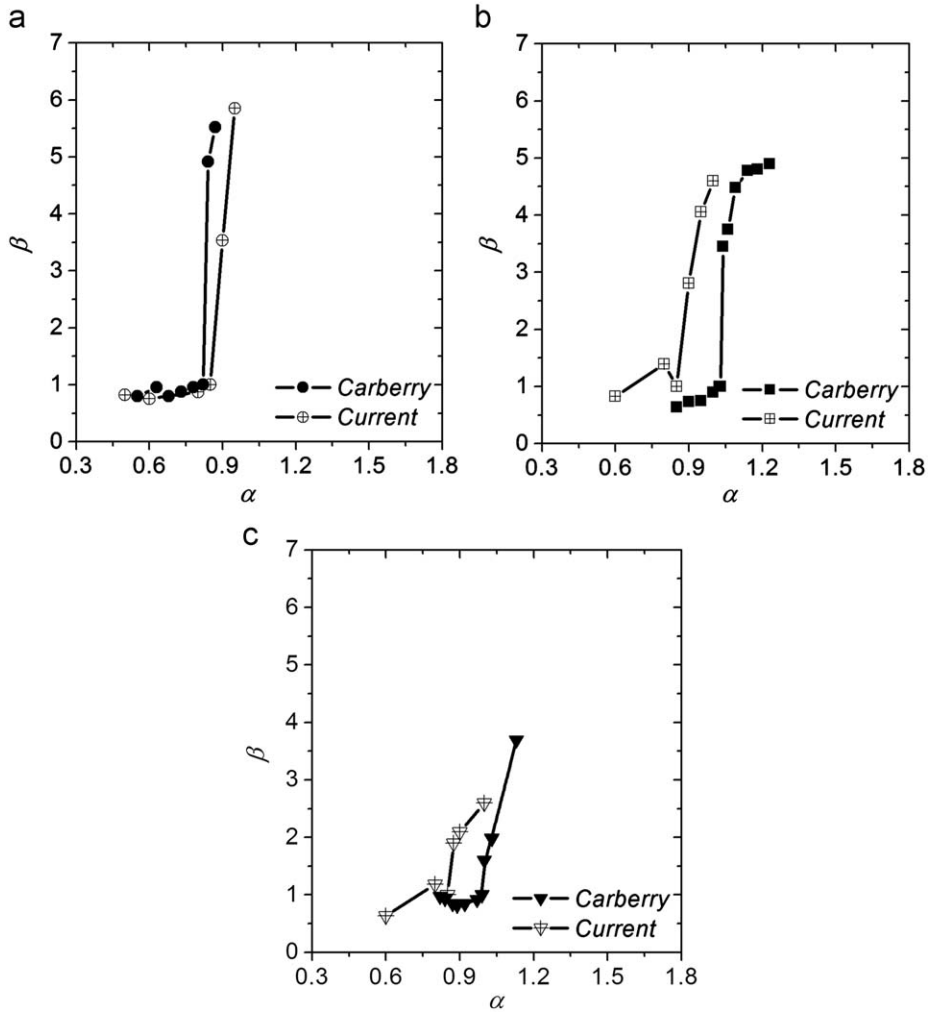

Fig. 7. (a) Lift jump ratio at *Re*=2300, (b) lift jump ratio at *Re*=4410 and (c) lift jump ratio at *Re*=9100.

Table 3
Comparison of the jump ratios.

Re	2300	4410	9100
Experiment results	5.52	4.48	1.98
Numerical results	5.85	4.60	2.09

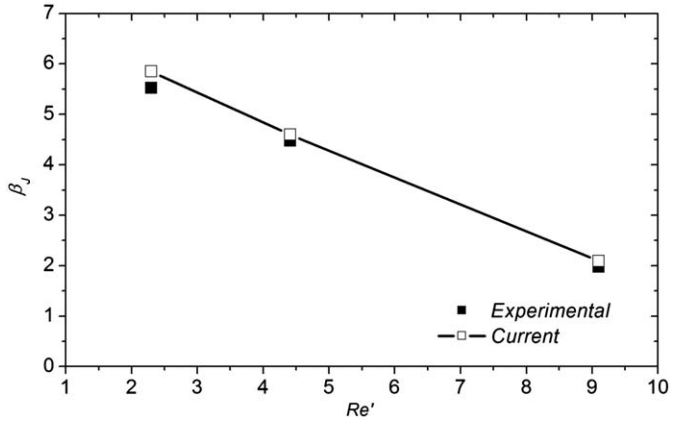

Fig. 8. The comparison in numerical results and experimental data.

force trace on the lift and drag coefficients plane, it is found that the lift coefficient has more contribution to the incensement of the maximum fluid resultant than the drag. Generally speaking, the jump ratio decreases as the Reynolds number increases. Using a simple linear fitting, a model easy-to-use for predicting jump of lift force is established properly comparing to the experimental data. The Reynolds number scope of application of this model is prescribed to be 2300–9100 by the case study.

Although the cylinder motion is set to be a sinusoidal form, the characteristics of the fluid force coefficients variation in forced oscillation situation have certain similarity in the lift amplitude with the one of vortex induced vibration of a freely oscillating pipeline: the low-frequency state is supposed to the lower branch and the high-frequency state is equivalent to the initial branch of structural response in VIV. However, the phase of lift and drag does not meet the law. A lot of experiments, including physical and numerical, are still needed to reveal the conditions under which the forced oscillation can be used to simulate the VIV cases.

Acknowledgements

This research was sponsored by the NSFC (Grant no. 40776057), the project of MOST (Grant no. 2006AA09Z301) and the project of CAS (KZCX2-YW-212-2). They are gratefully acknowledged.

References

Anagnostopoulos, P., 2000. Numerical study of the flow past a cylinder excited transversely to the incident stream. Part 1: lock-in zone, hydrodynamic forces and wake geometry. Journal of Fluids and Structures 14, 819–851.

Carberry, J., Sheridan, J., Rockwell, D., 2005. Controlled oscillations of a cylinder: forces and wake modes. Journal of Fluid Mechanics 538, 31–69.

Gopalkrishnan, R., 1993. Vortex-induced forces on oscillating bluff cylinders. Ph.D. Thesis, MIT, Cambridge, MA.

Govardhan, R., Wiliamson, C.H.K., 2000. Modes of vortex formation and frequency response for a freely-vibrating cylinder. Journal of Fluid Mechanics 420, 85–130.

Jamal, H.Al., Dalton, C., 2005. The contrast in phase angles between forced and self-excited oscillations of a circular cylinder. Journal of Fluids and Structures 20, 467–482.

Kaiktsis, L., Triantafyllou, G.S., Ozbas, M., 2007. Excitation, inertia, and drag forces on a cylinder vibrating transversely to a steady flow. Journal of Fluids and Structures 23, 1–21.

Leontini, J.S., Thompson, M.C., Hourigan, K., 2005. Modeling vortex-induced vibration with driven oscillation. Australian and New Zealand Industrial and Applied Mathematics Journal 46 (E), 365–378.

Lu, X.Y., Dalton, C., 1996. Calculation of the timing of vortex formation from an oscillating cylinder. Journal of Fluids and Structures 10, 527–541.

Sarpkaya, T., 1978. Fluid forces on oscillating cylinders. Journal of Waterway Port Coastal and Ocean Division-ASCE 104, 275–290.

Sarpkaya, T., 1995. Hydrodynamic damping, flow-induced oscillations, and biharmonic response. Journal of Offshore Mechanics and Arctic Engineering – Transactions of the ASME 117, 232–238.

Staubli, T., 1983. Calculation of the vibration of an elastically-mounted cylinder using experimental data from forced oscillation. Journal of Fluids Engineering – Transactions of the ASME 105, 225–229.

Zhang, Z.S., Cui, G.X., Xu, C.X., 2008. The Theory and Application of the Large Eddy Simulation. Tsinghua University Press pp. 90–107.